SCN1A Gain of Function in Early Infantile Encephalopathy

Géza Berecki, PhD ●,[1]* Alexander Bryson, MD,[1]* Jan Terhag, PhD,[1] Snezana Maljevic, PhD,[1] Elena V. Gazina, PhD,[1] Sean L. Hill, PhD,[2] and Steven Petrou, PhD[1,3]

Objective: To elucidate the biophysical basis underlying the distinct and severe clinical presentation in patients with the recurrent missense *SCN1A* variant, p.Thr226Met. Patients with this variant show a well-defined genotype–phenotype correlation and present with developmental and early infantile epileptic encephalopathy that is far more severe than typical *SCN1A* Dravet syndrome.

Methods: Whole cell patch clamp and dynamic action potential clamp were used to study T226M Na$_v$1.1 channels expressed in mammalian cells. Computational modeling was used to explore the neuronal scale mechanisms that account for altered action potential firing.

Results: T226M channels exhibited hyperpolarizing shifts of the activation and inactivation curves and enhanced fast inactivation. Dynamic action potential clamp hybrid simulation showed that model neurons containing T226M conductance displayed a left shift in rheobase relative to control. At current stimulation levels that produced repetitive action potential firing in control model neurons, depolarization block and cessation of action potential firing occurred in T226M model neurons. Fully computationally simulated neuron models recapitulated the findings from dynamic action potential clamp and showed that heterozygous T226M models were also more susceptible to depolarization block.

Interpretation: From a biophysical perspective, the T226M mutation produces gain of function. Somewhat paradoxically, our data suggest that this gain of function would cause interneurons to more readily develop depolarization block. This "functional dominant negative" interaction would produce a more profound disinhibition than seen with haploinsufficiency that is typical of Dravet syndrome and could readily explain the more severe phenotype of patients with T226M mutation.

ANN NEUROL 2019;85:514–525

Mutations in the *SCN1A* gene result in a wide spectrum of clinical phenotypes, from relatively mild generalized epilepsy with febrile seizures plus (GEFS+) to Dravet syndrome,[1,2] a treatment-resistant and life-threatening developmental and epileptic encephalopathy primarily caused by *SCN1A* loss of function. *SCN1A* mutations associated with Dravet syndrome are mostly truncating or missense, but other genetic changes have been documented.[3] In addition to seizures, Dravet patients also present with a range of comorbidities, including motor and speech delay, cognitive impairment, and behavioral difficulties.[4] The various clinical

phenotypes associated with any one *SCN1A* mutation are presumably influenced by genetic background.[2,3,5]

SCN1A encodes the voltage-gated Na$_v$1.1 channel that plays crucial roles in the generation and propagation of action potentials and exhibits dominant interneuron-specific expression.[6–8] Na$_v$1.1 channels are expressed in GABAergic interneurons in the neocortex, hippocampus, cerebellum, and main olfactory bulb.[9] At a subcellular level, Na$_v$1.1 channels cluster in the axon initial segments (AISs) of parvalbumin (PV)-positive interneurons and show moderate expression in the cell bodies of interneurons.[10] It has been proposed that

Na$_v$1.1 loss of function impairs the ability of GABAergic interneurons to fire action potentials at high frequency, thereby reducing postsynaptic GABA$_A$ receptor activation and leading to disinhibition of cortical pyramidal neurons.[7,11] This "loss of function" hypothesis has been successfully tested in a series of experiments using mouse models of Dravet syndrome.[3,12,13] It has also been demonstrated that reduced sodium current in cerebellar Purkinje neurons may be sufficient to cause ataxia,[14] whereas in other GABAergic neurons it may lead to different comorbidities.[15]

The T226M Na$_v$1.1 channel mutation[16] was identified in 8 unrelated children with profound developmental and epileptic encephalopathy (DEE) that was phenotypically distinct from Dravet syndrome.[17] T226M is recurrent and shows a fairly uniform clinical presentation, suggesting that a unique biophysical mechanism underlies this highly penetrant trait.[17] Understanding the biophysical consequences of this variant is important for revealing underlying pathology and devising treatment strategies. Because T226M mutation affects a conserved threonine residue in the S4 segment of domain I, it is likely to be associated with severe biophysical changes and consequently patient phenotypes.[18]

In this study, we used voltage clamp analyses to determine the biophysical properties of the T226M Na$_v$1.1 channel and real-time dynamic clamp[19] and computational modeling approaches to predict the impact of the mutation on neuronal firing activity. The V1353L Na$_v$1.1 channel variant, previously associated with GEFS+[20] and characterized as nonfunctional,[21] was also studied as a comparator. Our analyses revealed small differences between the firing properties of model neurons incorporating V1353L and wild-type variants. T226M channels exhibited dramatic changes in both activation and inactivation kinetics compared to wild type. We identified a unique epileptogenic mechanism due to T226M mutation resulting in enhanced susceptibility to depolarization block. This study also highlights the value of dynamic action potential clamp for efficiently predicting the impact of a complex ion channel dysfunction on neuronal activity.

Subjects and Methods

SCN1A Mutagenesis and Sequence Alignments
In our study, we refer to previously published patient data, for which Sadleir and colleagues reported ethics committee approval[17] as well as informed consent for each patient from parents or legal guardians. The human wild-type *SCN1A* cDNA (National Center for Biotechnology Information [NCBI] reference sequence [RefSeq] NM_001165963.2), encoding type I voltage-gated Na$_v$1.1 channel isoform 1 (NCBI RefSeq NP_001159435.1), cloned into the cytomegalovirus plasmid (pCMV), was a kind gift from Dr A. L. George Jr (Department of Pharmacology, Northwestern University). We modified the wild-type *SCN1A* sequence in the plasmid to reduce toxicity

and spontaneous mutagenesis in bacteria, without introducing any changes in the protein sequence. DNA synthesis (GenScript, Piscataway, NJ) was used to replace large segments of *SCN1A* cDNA with sequences containing numerous silent mutations, resulting in increased DNA stability during bacterial expression. The Supplementary Material includes the coding sequence of the modified *SCN1A* cDNA (Supplementary Fig S1), the alignment of the modified *SCN1A* sequence against the original *SCN1A* (NM_001165963.2; Supplementary Appendix 1), and the alignment of the unaltered protein sequence (RefSeq NP_001159435.1) encoded by either the original or the modified cDNA sequence (Supplementary Appendix 2). The V1353L and T226M mutations were introduced u*sing the QuikChange Lightning* Site-Directed Mutagenesis Kit (Agilent Technologies, Santa Clara, CA). All clones were verified by automated DNA sequencing (Australian Genome Research Facility, Melbourne, Victoria, Australia). Amino acid sequences of d*omain I* voltage sensors of h*uman SCN1A (*NP_001159435.1), *SCN2A* (NP_066287.2), *SCN3A* (NP_008853.3), *SCN4A* (NP_000325.4), *SCN5A* (AAI44622.1), *SCN8A* (NP_055006.1), *SCN9A* (NP_002968.1), and *SCN10A* (NP_006505.3) *were aligned* using the *CLC Sequence Viewer* 7.7 (Qiagen, Aarhus, Denmark).

Cell Culture and Heterologous Expression of Nav1.1 Channels
Chinese hamster ovary (CHO) cells were cultured, transiently cotransfected with plasmids encoding Na$_v$1.1 channel variant (4 μg) and enhanced green fluorescent protein (1 μg; Clontech, Mountain View, CA), and incubated as previously described.[19]

Electrophysiology
Electrophysiological recordings were performed 48 to 72 hours post-transfection at room temperature ($24 \pm 0.5°C$), using an Axopatch 200B amplifier (Molecular Devices, Sunnyvale, CA) controlled by a pCLAMP 9/DigiData 1440 acquisition system (Molecular Devices). The ionic compositions of the extracellular and intracellular solutions were identical to those described previously.[19] Borosilicate patch electrodes (GC150TF-7.5; Harvard Apparatus, Holliston, MA) typically exhibited resistance values of 1.2 to 1.5MΩ. Precautions were taken to minimize possible voltage errors, and cells exhibiting peak whole cell sodium currents (I$_{Nav1.1}$) smaller than 2 nA or exceeding 10 nA were excluded from analysis, as previously described.[19] Leak and capacitive currents were corrected using a −P/4 pulse except when determining steady-state inactivation and recovery from inactivation. Currents and potentials were low-pass filtered at 10 kHz and digitized at 50 kHz. Data were analyzed offline using Clampfit 9.2 (Molecular Devices) and Origin 9.0 (Microcal Software, Northampton, MA). Specific voltage-clamp protocols, assessing the current–voltage relationships, channel activation, inactivation, and recovery from inactivation are depicted in Figure 1 and explained in Results. Various biophysical parameters, including peak I$_{Nav1.1}$, membrane potential for half-maximal activation and inactivation (V$_{0.5,act}$ and V$_{0.5,inact}$, respectively), conductance, and time constants of activation/inactivation and recovery from fast inactivation were determined as previously described.[19,22]

Dynamic Action Potential Clamp

Our dynamic clamp configuration is identical to that described previously.[19] Briefly, heterologously expressed $Na_v1.1$ channel currents (input $I_{Na1.1}$) were incorporated into a biophysically realistic model of the distal AIS compartment. For all variants, peak input $I_{Na1.1}$ was scaled to a magnitude similar to that of
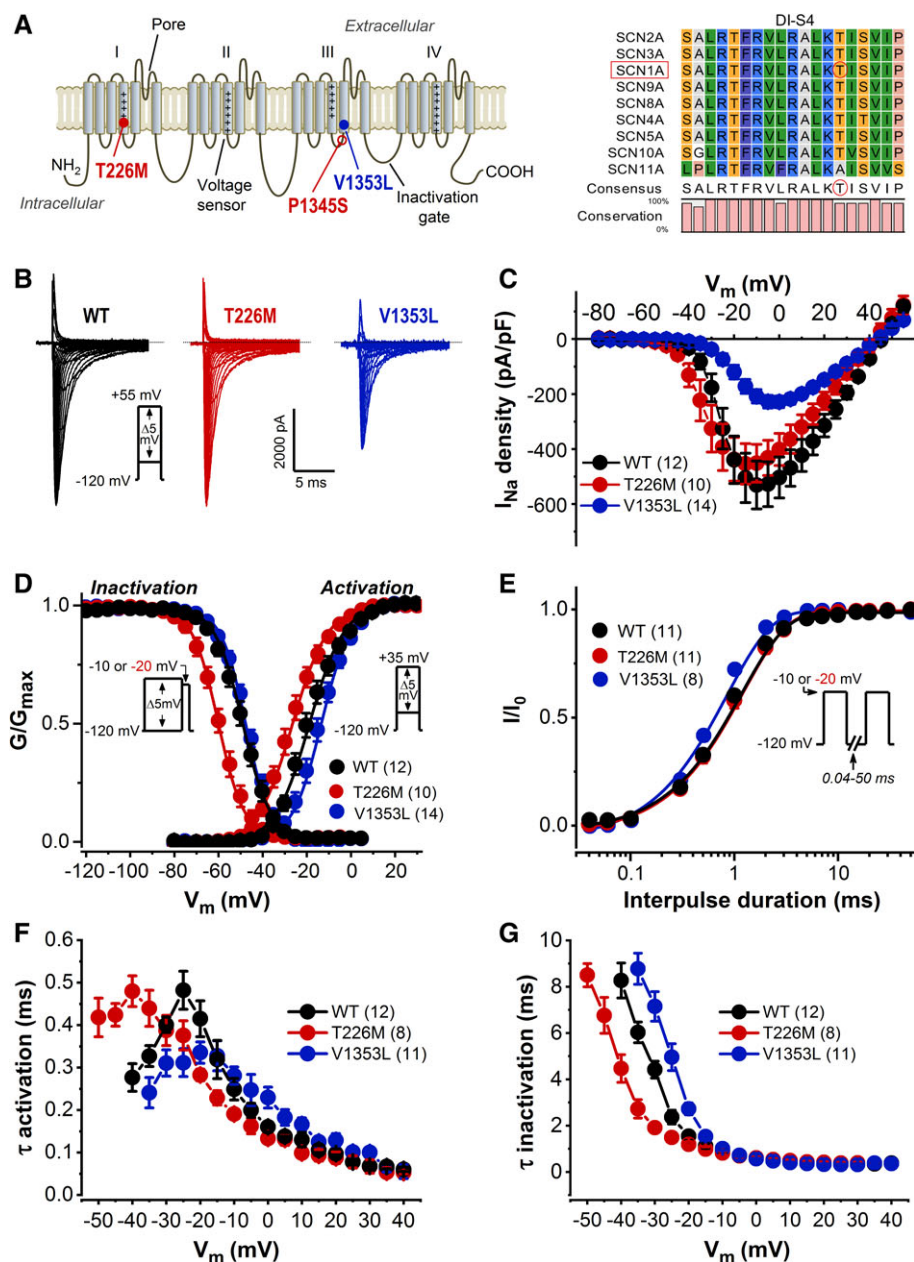

FIGURE 1: $Na_v1.1$ channel topology and biophysical properties of wild-type (WT), T226 M, and V1353 L channels. (A) Location of the T226M and V1353L mutations (left); the previously reported de novo missense P1345S variant[17] is also shown *(open circle)*. P1345S affects a highly conserved proline and results in profound developmental and epileptic encephalopathy similar to T226 M. The 4 membrane domains are marked I—IV; note the positive charges on segment 4 (S4) of each domain. Right: S4 sequence alignments of domain I (DI) in various human sodium channels; note the consensus sequence and the percentage of conservation; the conserved threonine is marked by a red circle (see also threonine position 226 in *SCN1A*); gating charge residues are shaded blue. (B) Representative wild-type and mutant $I_{Na1.1}$ traces, elicited by 20-millisecond depolarizing voltage steps of 5 mV increments from a holding potential (HP) of −120 mV. Inset: voltage protocol. (C) Peak $I_{Nav1.1}$ density–voltage relationships resulting from experiments shown in B. (D) Voltage dependence of activation and inactivation. Normalized conductance–voltage relationships, plotted as G/G_{max} values versus voltage, were fitted using Boltzmann equations (see parameters of the fits in the Table). Insets show the voltage protocols to assess activation and inactivation (see Subjects and Methods for details). (E) Recovery from inactivation, determined with a paired-pulse protocol from an HP value of −120 mV *(inset)*. Normalized peak $I_{Nav1.1}$ values (I/I_0) are plotted as a function of interpulse duration. (F, G) Time constants of activation and, respectively, inactivation versus voltage. The number of experiments is shown in parentheses; statistical evaluation of data is included in the Table. V_m = membrane potential.

original sodium current in the model cell (~350pA), thus any differences between the variants are due to altered biophysical properties. Nevertheless, for every variant, we also tested the effect of systematically varied input, with $I_{Na1.1}$ reduced to ~60% or increased to ~120% relative to control (~350pA). The AIS compartment was modeled in Simulink (MathWorks, Natick, MA) and included $Na_v1.6$ channel sodium current, fast rectifying potassium current, synaptic current, passive leak current, and membrane capacitance (C_m). In dynamic clamp configuration, the input $I_{Nav1.1}$ partly or entirely replaces the original in silico sodium current of the model. The AIS compartment is in current clamp mode, and its membrane potential (V_m) is computed in real-time while the $Na_v1.1$ channel-expressing CHO cell is in voltage clamp mode. The command potential for the CHO cell is the computed free-running V_m of the AIS compartment. Previously, we have performed a comprehensive sensitivity analysis and evaluated the robustness of our AIS compartment model.[19] In this study, AIS model firing was elicited by 2 methods consisting of injecting step current (I_{st}) via the Clampex module or enabling scalable simulated excitatory and inhibitory synaptic inputs within the compartment model, as previously described.[19] In all experiments, we kept the AIS compartment model capacitance (C_m = 1.88 pF) and leak conductance (gLeak = 0.3nS) unchanged. When using step stimuli, we systematically varied the $Na_v1.6$ channel and K_v channel conductances (gNa$_v$1.6 and gK$_v$, respectively) between the following settings: gNa$_v$1.6 = 0 and gK$_v$ = 1; gNa$_v$1.6 = 0, gK$_v$ = 3; or gNa$_v$1.6 = 0.15, gK$_v$ = 3. To facilitate action potential firing, 15% of the original in silico gNa$_v$1.6 was coimplemented with the external input $I_{Nav1.1}$; the scaled gK$_v$ (3 times the original value) helped to efficiently repolarize the model cell's V_m and subsequently recover Na_v channels from inactivation.[19] In the experiments using the Ornstein–Uhlenbeck model of synaptic noise, the gNa$_v$1.6 was set to 0 or 0.15, whereas gKv was unchanged because gK$_v$ scaling produces relatively small changes in the firing frequency of the AIS compartment model in response to synaptic current stimulation.[19]

In Silico Neuron Modeling

The interneuron model was developed using the Blue Brain Project neocortical microcircuit portal.[23,24] It contains 11 voltage- and calcium-dependent conductances using channel kinetics as described previously.[25] In addition, the model includes either wild-type or mutant $Na_v1.1$ conductances with kinetics based on the results of the voltage clamp experiments shown in Figure 1 and the Table. Activation and inactivation were fitted with Boltzmann functions, and time constants were fitted using Gaussian functions as previously described.[19] Simulations assumed a temperature of 24°C. $I_{Nav1.1}$ was described using the Hodgkin–Huxley formulation:

$$I_{Nav1.1} = g_{Nav1.1} * m^3 * h(V - E_{Na})$$

where $g_{Nav1.1}$ represents the peak conductance, V is the membrane potential, E_{Na} is the Na$^+$ reversal potential, and m and h are the activation and inactivation gating variables, respectively.[26]

The peak conductance of each channel was optimized to fit electrophysiological features of an interneuron with "continuous nonaccommodating" characteristics.[27,28] This interneuron subtype was chosen because $Na_v1.1$ is thought to be expressed at higher levels in PV-positive interneurons, which typically exhibit nonaccommodating firing properties.[29,30] Model optimization was performed using BluePyOpt[24] on a supercomputing cluster available through the Blue Brain Project (https://bluebrain.epfl.ch/).

All model simulations and analyses were performed with NEURON and Python.[31,32] Input–output relationships were obtained by injecting current into the soma. Heterozygous or homozygous phenotypes were modeled by adjusting $Na_v1.1$ channel kinetics to the corresponding T226M values in 50 or 100% of the wild-type $Na_v1.1$ channels, respectively. Action potential amplitude and half-width were determined as previously described.[19] The sensitivity analysis was performed by varying $V_{0.5,act}$ and $V_{0.5,inact}$ in 50% of the optimized $Na_v1.1$ channels (ie, the heterozygous model) in each compartment and recalculating the input–output relationship. Midpoints of the Gaussian fits to time constants of activation/inactivation were shifted from the wild-type value in proportion to the shift in $V_{0.5}$ value. Peak firing frequency refers to the maximum frequency elicited before onset of depolarization block. In the wild-type model, the impact of $Na_v1.1$ peak conductance on firing frequency was explored using an identical approach, but instead varying $g_{Nav1.1}$.

Statistical Analysis

Statistical comparison between $Na_v1.1$ channel variants was performed using 1-way analysis of variance (ANOVA) followed by Tukey post hoc test.

Two-way ANOVA was used for comparing the firing frequencies in the presence of various $Na_v1.1$ channels. Differences were considered significant if $p < 0.05$.

Results

We examined the biophysical properties of wild-type, T226M, and V1353L $Na_v1.1$ channel variants using whole cell patch clamp in CHO cells. Peak sodium current and current density in cells expressing T226M were similar to wild type (see Fig 1 and Table). The voltage dependence of activation and inactivation were severely affected by the T226M mutation, resulting in 8.1 and 11.4mV shifts for the $V_{0.5,act}$ and $V_{0.5,inact}$, respectively, toward hyperpolarizing potentials. From a functional standpoint, these shifts are consistent with gain of function due to enhanced channel opening and loss of function due to stabilized inactivation. T226M channel recovery from fast inactivation was unaffected, whereas the activation and inactivation kinetics were changed. Notably, the time to peak current of T226M channels was slower at voltages more negative than −30 mV and fast inactivation was accelerated relative to wild type. These results suggest that T226M channels exhibit a mixed biophysical defect that could lead to either gain of function due to a hyperpolarizing shift of the activation curve, or loss of function due to the hyperpolarizing shift of the inactivation curve and shorter time course of inactivation. The GEFS+ variant, V1353L, was functionally characterized, and relative to wild type

displayed reduced current density and a ~5.5mV depolarizing shift of activation consistent with loss of function. It also displayed faster recovery from inactivation and a slower kinetics of inactivation, consistent with gain of function (Table).

The overall functional effect of T226M mutation cannot be intuitively predicted from the measured changes in biophysical characteristics. To provide a more objective measure of the excitability of neurons harboring the T226M variant, we implemented dynamic action potential clamp.[19] Figure 2 shows action potential firing of a "hybrid" cell comprising an in silico model cell and the conductance of either the wild-type or the T226M channels expressed in CHO cells. In addition, various levels of in silico $gNa_v1.6$ or gK_v were tested and the input–output properties determined in response to stepwise depolarizing I_{st}. Manipulation of in silico $Na_v1.6$ or K_v conductances provides a better understanding of the range of firing properties of the model neuron. For each conductance level, we determined the effect of the mutation on firing and plotted the input–output relationships, representing the mean number of action potentials as a function of I_{st}. Analysis of a wild-type model with values of $gNa_v1.6 = 0$ and $gK_v = 1$ resulted in relatively low firing. As seen in our previous dynamic clamp study,[19] action potential firing could be increased using a gK_v setting of 3 or by simultaneously adjusting $gNa_v1.6$ and gK_v to 0.15 and 3, respectively, relative to the conductance level in Figure 2A ($gNa_v1.6 = 0$ and $gK_v = 1$). When the hybrid neuron included in silico $gNa_v1.6$ (scaled by 0.15), hybrid cell firing rate increased and rheobase decreased. Relative to the action potential firing seen in cells expressing wild-type channels, there was a significant left shift in the input–output curve in cells expressing T226M channels, indicating enhanced excitability. Critically, action potential firing collapse was seen in cells expressing T226M at stimulus levels where normal firing was seen in the wild-type–expressing cells, consistent with a marked reduction in excitability. This reduced firing is caused by the development of depolarization block, where the expression and activation of the T226M channels causes a gradual shift in the baseline V_m. Such depolarization block typically occurs at high levels of stimulus current in wild type; however, the presence of the T226M channel shifts this point of collapse to much lower stimulus levels and is likely to be a major contributor of the pathology in these patients.

The rheobase of V1353L channels was similar to wild type in dynamic clamp experiments performed as above. I_{st} values between 4 and 12pA elicited slightly reduced action potential firing with V1363 L variant compared to wild type, whereas this effect diminished in the presence of $gNa_v1.6$ (see Fig 2). With a gK_v setting of 3, I_{st} values above ~22pA resulted in higher firing, likely due to more efficient recovery from inactivation of the V1363 L variant compared to wild type.

The impact of T226M or V1353L variant on AIS model cell firing was also probed in response to scaled excitatory (g_e) to inhibitory (g_i) conductance ratios mimicking synaptic stimuli of various intensity in dynamic action potential clamp mode (Fig 3). These experiments were undertaken using fixed levels of $gNa_v1.6 = 0.15$ and $gK_v = 1$ conductance levels. Hybrid neurons incorporating wild-type $I_{Nav1.1}$ did not show activity with a $g_e:g_i$ ratio of 1, whereas higher $g_e:g_i$ ratios initiated firing that reached a maximum with a $g_e:g_i$ ratio of 3 and then abruptly decreased. Relative to wild type, hybrid neurons incorporating T226M showed a reduced rheobase, exhibited high-frequency action potential firing with $g_e:g_i$ ratios between 0 and 2, and exhibited diminished action potential firing above a $g_e:g_i$ ratio of 2. These results further validate the T226M variant's profile, characterized by low stimulation strength, enhanced excitability, and subsequent depolarization block induced by stimulation strength that would cause optimal activation in wild type. Relative to wild type, the V1363 L variant resulted in a reduced action potential firing with $g_e:g_i$ ratios of 2 and 3.

We also investigated the impact of the T226M mutation on neuronal excitability using a biophysically detailed computational model of a PV-positive cortical interneuron (Fig 4). $Na_v1.1$ channel kinetics were modeled using results from the voltage clamp analysis (see Figs 1 and 4A, Table). We first examined the role of $N_{av1.1}$ channel density ($g_{Nav1.1}$) upon firing properties in the wild-type model. Consistent with previous experimental observations,[29] increased $g_{Nav1.1}$ values reduced action potential width at base and sustained higher frequency firing. Small increases in action potential height were also observed (see Fig 4). We then obtained the input–frequency relationships of PV interneurons "expressing" wild-type or T226M $Na_v1.1$ channels (thus modeling the homozygous phenotype). Depolarization block in the T226M variant occurred at an I_{st} value of 0.16 nA (corresponding to 40% of wild-type I_{st}) and was unable to sustain firing frequencies >95 Hz. Next, we specifically asked whether 50% of T226M variant contribution to total $g_{Nav1.1}$ (thus mimicking the heterozygous phenotype) would impact model behavior relative to wild type. In the heterozygous model, firing frequencies >125 Hz could not be sustained, and depolarization block occurred at an I_{st} value of 0.28 nA. This value corresponds to 70% of the I_{st} producing depolarization block in the wild type (0.4nA). This observation suggests a "functional dominant negative" mechanism whereby the T226M channel can reduce the activity of wild-type channel in the absence of direct protein–protein interaction. This is consistent with
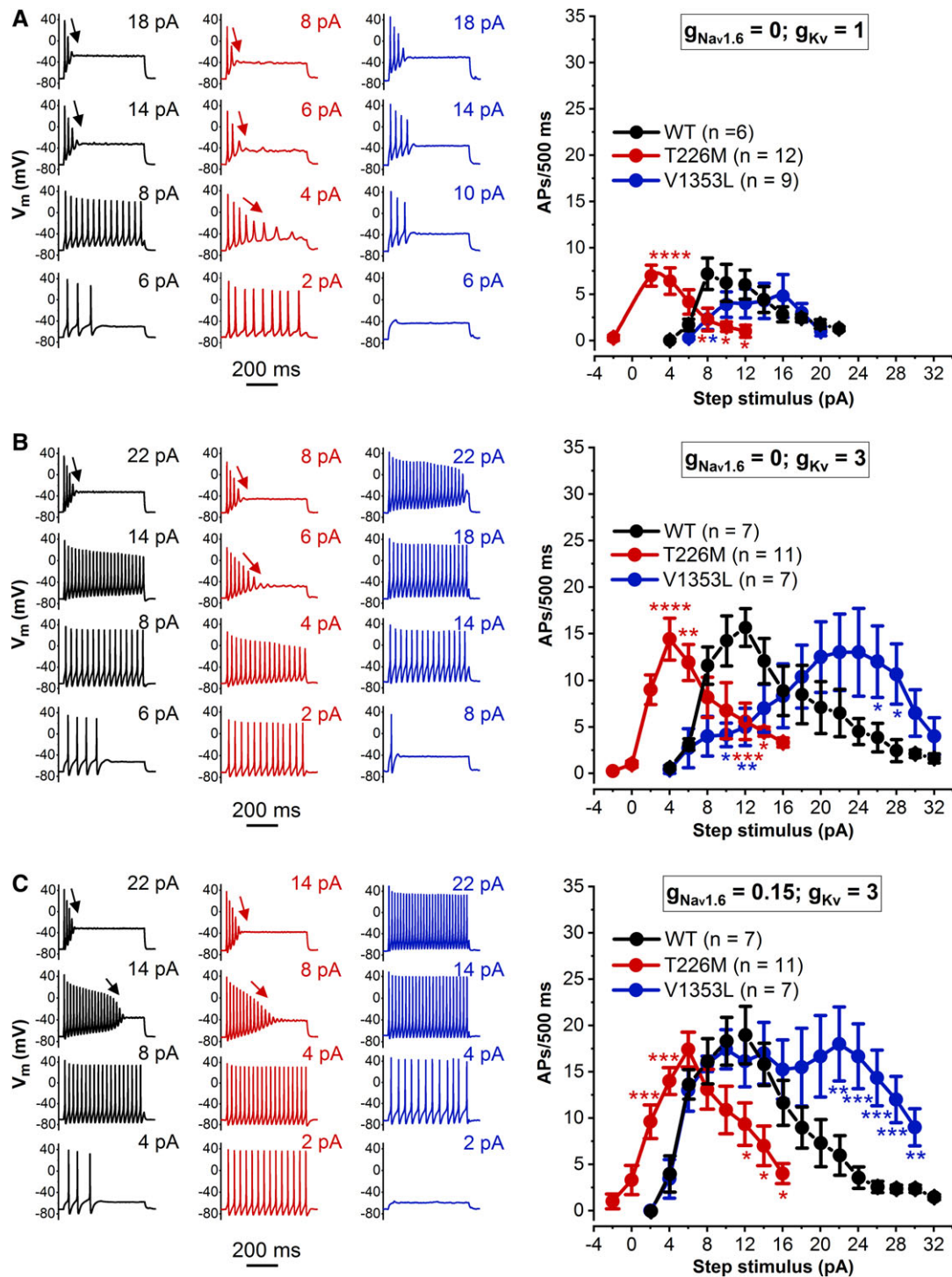
FIGURE 2: Dynamic action potential-clamp experiment implementing wild-type (WT), T226M, or V1353L $I_{Nav1.1}$. Input–output relationships were obtained by using 3 distinct K_v and $Na_v1.6$ conductance settings in the axon initial segment model cell: $gK_v = 1$, $gNa_v1.6 = 0$ (A); $gK_v = 3$, $gNa_v1.6 = 0$ (B); and (C) $gK_v = 3$, $gNa_v1.6 = 0.15$. Left: representative membrane potential (V_m) traces and the corresponding step current (I_{st}) values. In all experiments, V_m changes were elicited by I_{st} of 500-millisecond duration, in 2pA increments. Arrows indicate depolarization block. Data are mean ± standard error of the mean; number of experiments is given in parentheses. *$p < 0.05$, **$p < 0.01$, ***$p < 0.001$, ****$p < 0.0001$ compared to WT, 2-way analysis of variance with Tukey post hoc test. AP = action potential.

the observation that these patients are significantly more impacted than in Dravet syndrome, where variants typically cause haploinsufficiency alone[33] without this additional functional dominant negative interaction. The T226M variant had no effect on rheobase in either model, likely due to the presence of other Na_v subtypes (see Discussion).
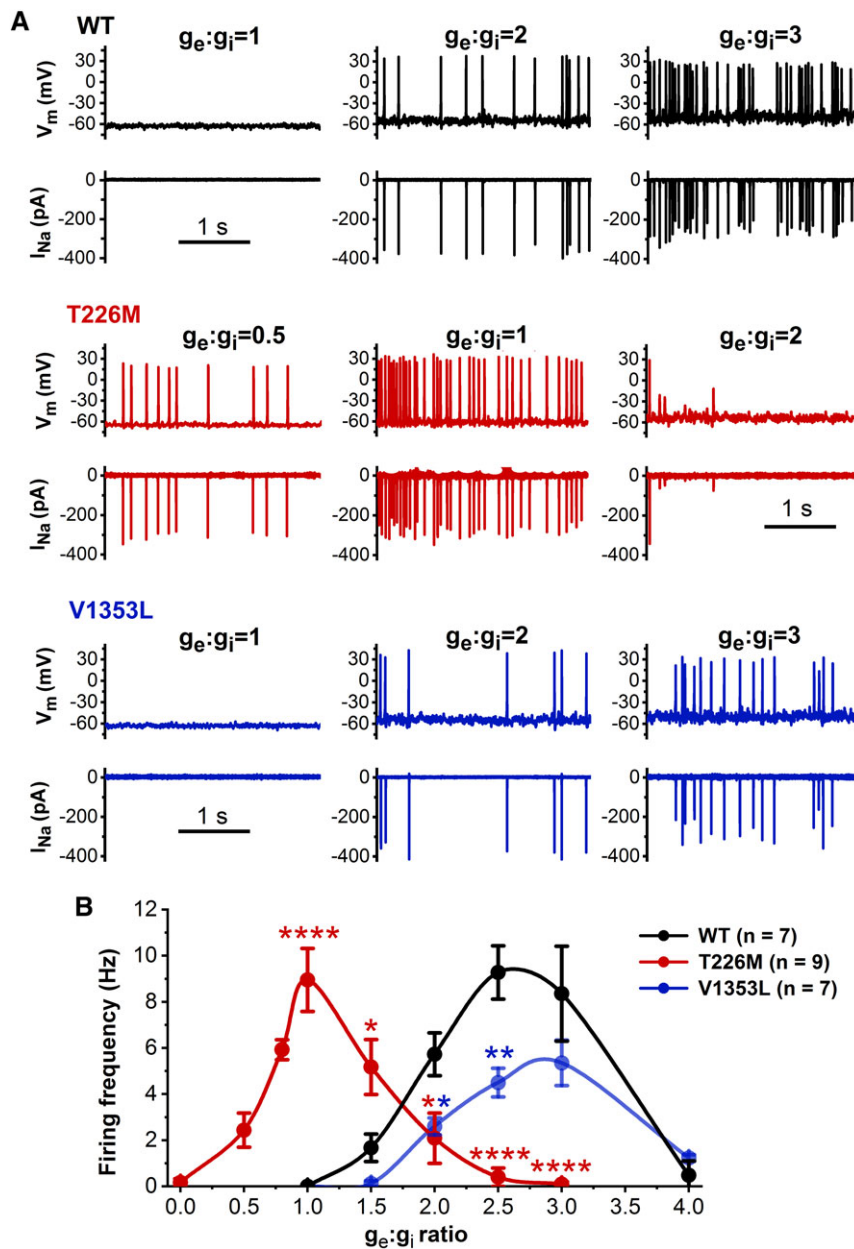
FIGURE 3: Firing of the axon initial segment model cell incorporating wild-type (WT), T226M, or V1353L $I_{Nav1.1}$ in response to scaled synaptic conductance input. (A) Typical firing responses with various excitatory conductance (g_e) to inhibitory conductance (g_i) ratio values. Membrane potential (V_m) changes (upward deflections) and associated scaled input $I_{Nav1.1}$ traces (downward deflections) are shown. (B) Input–output relationships in the model cell as a function of g_e:g_i. Data are mean ± standard error of the mean; number of experiments is given in parentheses. *$p < 0.05$, **$p < 0.01$, ****$p < 0.0001$ compared to WT, 2-way analysis of variance with Tukey post hoc test.

Both models clearly demonstrated depolarization block with lower levels of stimulating current as compared to wild type.

Finally, we performed a sensitivity analysis to obtain insight into the differential roles of $V_{0.5,act}$ and $V_{0.5,inact}$ on peak firing frequency and depolarization block (Fig 5). This is of interest because changes in these parameter values appear to be pathogenic. At a given $V_{0.5,act}$, shifting $V_{0.5,inact}$ to more depolarized values enabled progressively higher peak frequencies, until a threshold was reached whereby the model was

unable to sustain repetitive action potentials due to overwhelming depolarizing current. This is consistent with a previous study showing that depolarization block is critically dependent upon activation and inactivation $V_{0.5}$.[34] Interestingly, the highest firing frequencies were observed when both $V_{0.5,act}$ and $V_{0.5,inact}$ were shifted by a similar amount toward more depolarized values. In the T226M mutation, the opposite occurs; both values are shifted to more hyperpolarized values, moving the behavior of the system to a region where high-frequency firing cannot be sustained.
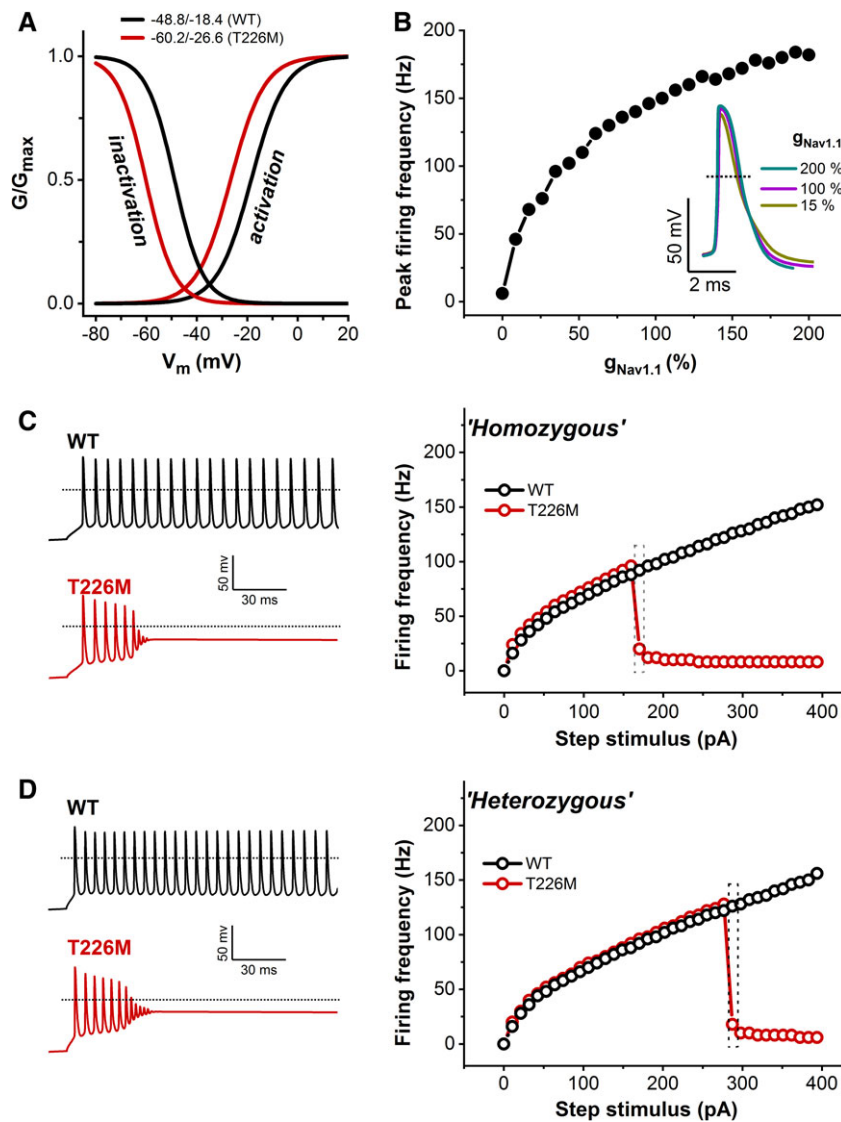
FIGURE 4: Action potential firing of the parvalbumin (PV)-positive interneuron model incorporating wild-type (WT) and/or T226M $g_{Nav1.1}$. (A) Normalized G/G_{max} relationships of the homozygous models; the half-maximal activation ($V_{0.5,act}$) and half-maximal inactivation ($V_{0.5,inact}$) values for each $Na_v1.1$ variant are shown (top). In the heterozygous T226M model, the $V_{0.5,act}$ and $V_{0.5,inact}$ were shifted by −4.1 and − 6 .5mV, respectively, relative to WT (not shown). (B) Impact of scaled WT $g_{Nav1.1}$ on peak firing frequency. Each value corresponds to the maximum firing frequency that can be sustained before depolarization block occurs. Inset shows typical action potential morphology with $g_{Nav1.1}$ scaled to 15, 100, or 200%; dotted line indicates zero membrane potential (V_m). For all simulations shown below, 100% $g_{Nav1.1}$ was used. (C, D) Input–output relationships in the PV interneuron model incorporating WT or T226M $g_{Nav1.1}$ alone (homozygous; C), and WT and T226M $g_{Nav1.1}$ at a 1:1 ratio (heterozygous; D). In all cases, firing was elicited by a step current of 1-second duration, in 10pA increments. Left: Representative V_m traces demonstrating firing corresponding to the boxed areas from C and D and depolarization block due to T226M $g_{Nav1.1}$; for clarity, only ~150 milliseconds of the 1-second V_m traces are shown. Note that depolarization block occurs at lower stimulus amplitude in the homozygous model compared to the heterozygous model.

Taken together, our results suggest that the main impact of the T226M mutation is early enhanced excitability followed by early depolarization block. These functional deficits may underlie the pathophysiology in patients harboring this mutation.

Discussion

SCN1A is one of the most clinically relevant epilepsy genes.[35] Typically, de novo missense mutations and truncations

leading to *SCN1A* loss of function are associated with Dravet syndrome. It has been proposed that the severity of loss of function correlates with disinhibition of GABAergic interneurons.[7] In a comprehensive clinical study, a recurrent de novo missense *SCN1A* mutation, p.Thr226Met, showed a distinctive genotype–phenotype correlation and resulted in a developmental and epileptic encephalopathy that was clearly distinguished from Dravet syndrome.[17] Affected patients presented with pharmacoresistant early onset hemiclonic seizures
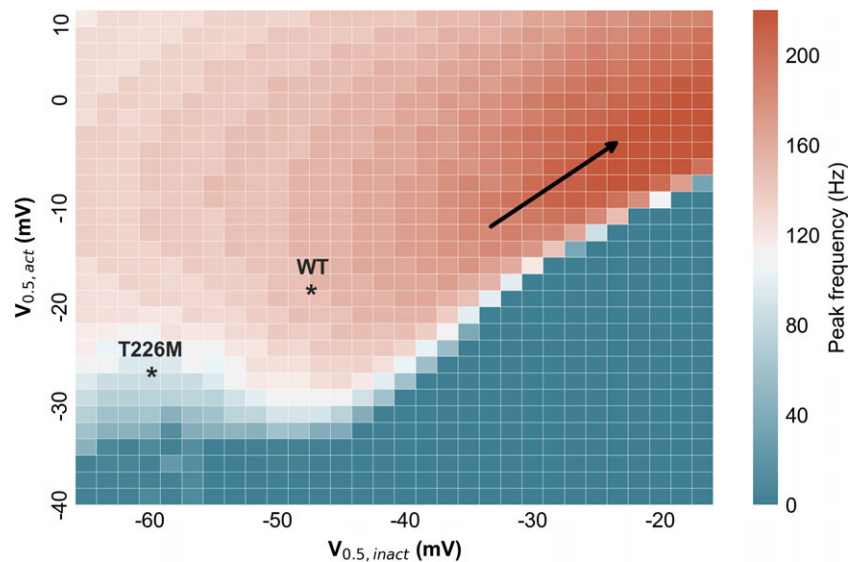
FIGURE 5: Impact of $Na_v1.1$ $V_{0.5,act}$ (y-axis) and $V_{0.5,inact}$ (x-axis) upon peak frequency (color-coded) prior to depolarization block for wild-type (WT) and T226M channels. At a given half-maximal activation ($V_{0.5,act}$), shifting half-maximal inactivation ($V_{0.5,inact}$) toward depolarized values leads to progressively higher peak frequencies until depolarization block (area marked by blue–gray) occurs. This corresponds to greater separation between activation/inactivation curves ("window" current). Maintaining this window current while shifting to more depolarized potentials *(black arrow)* generates progressively higher peak frequencies.

occurring at a mean age of 9 weeks and tonic–clonic seizures by 18 months; additional symptoms included developmental delay, intellectual disability, and prominent movement disorder.[17] Because Dravet syndrome is often caused by simple haploinsufficiency, the mechanism by which the T226M mutation produces a more severe phenotype is of interest. The most parsimonious explanation is dominant negative interaction that by its nature would be more profound than simple haploinsufficiency. In sodium channels, dominant negative interactions can occur via "physical" homomeric interaction[36] or by "functional" interaction whereby the mutant channel alters membrane potential in a way that reduces availability of the wild-type channel.

In this study, we explored whether functional dominant negative interactions could underlie the severity of clinical presentation in patients with the recurrent T226M $Na_v1.1$ channel mutation. Voltage clamp analysis suggested that the T226M variant exhibits mixed biophysical characteristics. The hyperpolarizing shift in voltage dependence of activation can cause enhanced action potential firing,[37] whereas the left shift in the voltage dependence of inactivation is consistent with loss of excitability. Such opposing changes make it difficult to intuitively predict the overall impact of the T226M mutation on neuronal excitability.

To overcome this difficulty, we implemented dynamic action potential clamp to determine the impact of wild-type or mutant $I_{Nav1.1}$ upon the excitability of a single compartment neuronal model. The T226M variant significantly reduced the rheobase, suggesting enhanced excitability. However, firing could not be sustained, and

depolarization block was evident at stimulation levels near rheobase of wild-type *SCN1A*-containing neurons. This suggests that at "low" levels of synaptic input, T226M enhances PV interneuron activity, whereas disinhibition and overexcitation predominate at "typical" levels that otherwise cause regular firing of wild-type interneurons. This may be of importance for excitation–inhibition balance, because epileptic circuit motifs might switch rapidly from overinhibition at low input to overexcitation at high input, and could significantly contribute to the phenotype in these patients. PV interneurons, capable of mediating feedforward inhibition,[38] may be of particular importance in this context, and breakdown of epileptic circuit choke points could further drive ictal propagation.[39]

There is recent evidence that sodium channel α-subunits oligomerize and can form dimers,[36] opening the possibility that "structural" dominant negative interactions could occur due to such channel assembly. Our modeling studies also suggest that "functional" dominant negative interactions alone may be sufficient to produce neuronal disinhibition by enhanced sensitivity to depolarization block. This is relevant for PV-positive interneurons that exhibit sustained high-frequency firing that is unlikely to be supported by the T226M variant. The functional deficit caused by the T226M mutation, therefore, may have a greater impact in neurons displaying high-frequency firing typical of PV-positive interneurons given their high expression of $Na_v1.1$.

To better understand the diverse neurophysiological mechanisms due to *SCN1A* mutations, we also studied the

TABLE. Biophysical Parameters of I_{Na} through $Na_v1.1$ Channel Variants			
Biophysical Property	**Wild Type**	**T226M**	**V1353L**
Current density			
At −10 mV, pA/pF	530.5 ± 86.9	451.1 ± 68.8	208.0 ± 24.4[a]
n	12	10	14
Activation			
$V_{0.5,act}$, mV	−18.46 ± 0.71	−26.6 ± 0.64[b]	−13.0 ± 0.51[b]
k_{act}, mV	7.91 ± 0.25	8.00 ± 0.29	6.67 ± 0.23[a]
n	12	10	14
Inactivation			
$V_{0.5,inact}$, mV	−48.8 ± 0.66	−60.2 ± 0.50[b]	−47.4 ± 0.51
k_{inact}, mV	6.25 ± 0.28	5.85 ± 0.24	5.59 ± 0.28
n	12	10	14
Time course of activation			
τ at −35 mV, ms	0.32 ± 0.02	0.44 ± 0.04[c]	0.24 ± 0.03
τ at 0 mV, ms	0.16 ± 0.01	0.13 ± 0.01	0.22 ± 0.02[c]
n	12	8	11
Time course of fast inactivation			
τ at −30 mV, ms	4.41 ± 0.36	1.92 ± 0.20[a]	7.15 ± 0.64[d]
n	12	8	11
Time course of recovery from fast inactivation			
τ, ms	1.39 ± 0.10	1.45 ± 0.11	0.87 ± 0.06[a]
n	11	11	8

Data are represented as mean ± standard error of the mean.
[a] $p < 0.01$, [b] $p < 0.0001$, [c] $p < 0.05$, [d] $p < 0.001$ compared with wild-type, 1-way analysis of variance with Tukey post hoc test.
$k_{(in)act}$ = slope factor of steady-state (in)activation curve; n = number of cells; $V_{0.5,(in)act}$ = membrane potential for half-maximal (in)activation; τ = time constant;

V1353L variant identified in familial cases of GEFS+.[20,40] Phenotypes associated with the V1353L mutation are heterogeneous but, overall, less severe than typical Dravet cases.[20] A previous biophysical analysis of the V1353L variant resulted in nonfunctional channels in transiently transfected human embryonic kidney (tsA-201) cells. Remarkably, we were able to obtain functional expression of this variant in CHO cells. Our biophysical and dynamic clamp analyses showed a milder reduction in interneuron firing properties consistent with the milder presentation of this familial disorder. This, once again,[19,41] demonstrates the utility of the dynamic clamp method in providing strong physiological correlates of clinical severity for mutant sodium channels where opposing biophysical changes make intuitive interpretation difficult.

Paradoxically, T226M patients may benefit from sodium channel blockade that could reduce availability and thereby lessen the sensitivity to depolarization block.

Focal and multifocal epileptiform discharges were typically seen in the electroencephalographic recordings of T226M mutation carriers.[17] The basic molecular and cellular mechanisms of such epileptic events can be diverse and may include increased excitatory synaptic efficacy as well changes in intrinsic excitability of neurons.[42] It has been suggested that depolarization block correlates with focal activity during electrographic seizures,[43] which could drive multifocal discharges in the T226M patients.

Taken together, our data reveal an unusual biophysical mechanism for the T226M variant resulting in

neurons more susceptible to depolarization block. The network-scale impact of the T226M Na$_v$1.1 channel mutation requires further studies using more complex in silico models where the Na$_v$ channel variant-specific functional output of interneuron activity can be investigated. Genetically engineered animals and patient-derived induced pluripotent stem cell models expressing T226M will be invaluable to further elucidate the network and behavioral impact and help reveal molecular pathology associated with this severe phenotype and suggest therapeutic strategies to overcome this specific disease mechanism.

Acknowledgment

Author Contributions

G.B., A.B., S.L.H., and S.P. contributed to the conception and design of the study; G.B., A.B., J.T., S.M., and E.V.G. contributed to the acquisition and analysis of data; G.B., A.B., J.T., and S.P. contributed to drafting the text and preparing the figures.

Potential Conflicts of Interest

Nothing to report.

References

1. Claes L, Del-Favero J, Ceulemans B, et al. De novo mutations in the sodium-channel gene SCN1A cause severe myoclonic epilepsy of infancy. Am J Hum Genet 2001;68:1327–1332.

2. Mulley JC, Scheffer IE, Petrou S, et al. SCN1A mutations and epilepsy. Hum Mutat 2005;25:535–542.

3. Connolly MB. Dravet syndrome: diagnosis and long-term course. Can J Neurol Sci 2016;43(suppl 3):S3–S8.

4. Lagae L, Brambilla I, Mingorance A, et al. Quality of life and comorbidities associated with Dravet syndrome severity: a multinational cohort survey. Dev Med Child Neurol 2018;60:63–72.

5. Helbig I, Tayoun AA. Understanding genotypes and phenotypes in epileptic encephalopathies. Mol Syndromol 2016;7:172–181.

6. Rudy B, Fishell G, Lee S, Hjerling-Leffler J. Three groups of interneurons account for nearly 100% of neocortical GABAergic neurons. Dev Neurobiol 2011;71:45–61.

7. Catterall WA, Kalume F, Oakley JC. NaV1.1 channels and epilepsy. J Physiol 2010;588(pt 11):1849–1859.

8. Yamagata T, Ogiwara I, Mazaki E, et al. Nav1.2 is expressed in caudal ganglionic eminence-derived disinhibitory interneurons: mutually exclusive distributions of Nav1.1 and Nav1.2. Biochem Biophys Res Commun 2017;491:1070–1076.

9. Lorincz A, Nusser Z. Cell-type-dependent molecular composition of the axon initial segment. J Neurosci 2008;28:14329–14340.

10. Ogiwara I, Miyamoto H, Morita N, et al. Nav1.1 localizes to axons of parvalbumin-positive inhibitory interneurons: a circuit basis for epileptic seizures in mice carrying an Scn1a gene mutation. J Neurosci 2007;27:5903–5914.

11. Ragsdale DS. How do mutant Nav1.1 sodium channels cause epilepsy? Brain Res Rev 2008;58:149–159.

12. Han S, Tai C, Westenbroek RE, et al. Autistic-like behaviour in Scn1a +/- mice and rescue by enhanced GABA-mediated neurotransmission. Nature 2012;489:385–390.

13. Cheah CS, Yu FH, Westenbroek RE, et al. Specific deletion of NaV1.1 sodium channels in inhibitory interneurons causes seizures and premature death in a mouse model of Dravet syndrome. Proc Natl Acad Sci U S A 2012;109:14646–14651.

14. Kalume F, Yu FH, Westenbroek RE, et al. Reduced sodium current in Purkinje neurons from Nav1.1 mutant mice: implications for ataxia in severe myoclonic epilepsy in infancy. J Neurosci 2007;27:11065–11074.

15. Oakley JC, Kalume F, Catterall WA. Insights into pathophysiology and therapy from a mouse model of Dravet syndrome. Epilepsia 2011;52(suppl 2):59–61.

16. Harkin LA, McMahon JM, Iona X, et al. The spectrum of SCN1A-related infantile epileptic encephalopathies. Brain 2007;130(pt 3):843–852.

17. Sadleir LG, Mountier EI, Gill D, et al. Not all SCN1A epileptic encephalopathies are Dravet syndrome: early profound Thr226Met phenotype. Neurology 2017;89:1035–1042.

18. Zuberi SM, Brunklaus A, Birch R, et al. Genotype-phenotype associations in SCN1A-related epilepsies. Neurology 2011;76:594–600.

19. Berecki G, Howell KB, Deerasooriya YH, et al. Dynamic action potential clamp predicts functional separation in mild familial and severe de novo forms of SCN2A epilepsy. Proc Natl Acad Sci U S A 2018;115:E5516–E5525.

20. Wallace RH, Scheffer IE, Barnett S, et al. Neuronal sodium-channel alpha1-subunit mutations in generalized epilepsy with febrile seizures plus. Am J Hum Genet 2001;68:859–865.

21. Lossin C, Rhodes TH, Desai RR, et al. Epilepsy-associated dysfunction in the voltage-gated neuronal sodium channel SCN1A. J Neurosci 2003;23:11289–11295.

22. Sula A, Booker J, Ng LC, et al. The complete structure of an activated open sodium channel. Nat Commun 2017;8:14205.

23. Ramaswamy S, Courcol JD, Abdellah M, et al. The neocortical microcircuit collaboration portal: a resource for rat somatosensory cortex. Front Neural Circuits 2015;9:44.

24. Van Geit W, Gevaert M, Chindemi G, et al. BluePyOpt: leveraging open source software and cloud infrastructure to optimise model parameters in neuroscience. Front Neuroinform 2016;10:17.

25. Markram H, Muller E, Ramaswamy S, et al. Reconstruction and simulation of neocortical microcircuitry. Cell 2015;163:456–492.

26. Hodgkin AL, Huxley AF. A quantitative description of membrane current and its application to conduction and excitation in nerve. J Physiol 1952;117:500–544.

27. Druckmann S, Banitt Y, Gidon A, et al. A novel multiple objective optimization framework for constraining conductance-based neuron models by experimental data. Front Neurosci 2007;1:7–18.

28. Druckmann S, Berger TK, Schurmann F, et al. Effective stimuli for constructing reliable neuron models. PLoS Comput Biol 2011;7:e1002133.

29. Yu FH, Mantegazza M, Westenbroek RE, et al. Reduced sodium current in GABAergic interneurons in a mouse model of severe myoclonic epilepsy in infancy. Nat Neurosci 2006;9:1142–1149.

30. Markram H, Toledo-Rodriguez M, Wang Y, et al. Interneurons of the neocortical inhibitory system. Nat Rev Neurosci 2004;5:793–807.

31. Hines ML, Carnevale NT. The NEURON simulation environment. Neural Comput 1997;9:1179–1209.

32. Hines ML, Davison AP, Muller E. NEURON and Python. Front Neuroinform 2009;3:1.

33. Meisler MH, Kearney JA. Sodium channel mutations in epilepsy and other neurological disorders. J Clin Invest 2005;115:2010–2017.

34. Bianchi D, Marasco A, Limongiello A, et al. On the mechanisms underlying the depolarization block in the spiking dynamics of CA1 pyramidal neurons. J Comput Neurosci 2012;33:207–225.

35. International League against Epilepsy Consortium on Complex Epilepsies. Genetic determinants of common epilepsies: a meta-analysis of genome-wide association studies. Lancet Neurol 2014;13: 893–903.

36. Clatot J, Hoshi M, Wan X, et al. Voltage-gated sodium channels assemble and gate as dimers. Nat Commun 2017;8:2077.

37. Thomas EA, Reid CA, Berkovic SF, Petrou S. Prediction by modeling that epilepsy may be caused by very small functional changes in ion channels. Arch Neurol 2009;66:1225–1232.

38. Cammarota M, Losi G, Chiavegato A, et al. Fast spiking interneuron control of seizure propagation in a cortical slice model of focal epilepsy. J Physiol 2013;591:807–822.

39. Paz JT, Huguenard JR. Microcircuits and their interactions in epilepsy: is the focus out of focus? Nat Neurosci 2015;18:351–359.

40. Scheffer IE, Berkovic SF. Generalized epilepsy with febrile seizures plus. A genetic disorder with heterogeneous clinical phenotypes. Brain 1997;120(pt 3):479–490.

41. Berecki G, Zegers JG, Verkerk AO, et al. HERG channel (dys)function revealed by dynamic action potential clamp technique. Biophys J 2005;88:566–578.

42. Dichter MA, Ayala GF. Cellular mechanisms of epilepsy: a status report. Science 1987;237:157–164.

43. Bikson M, Hahn PJ, Fox JE, Jefferys JG. Depolarization block of neurons during maintenance of electrographic seizures. J Neurophysiol 2003;90:2402–2408.